Progress In Electromagnetics Research Letters, Vol. 46, 49–57, 2014

Space-Borne Hexagonal Array Element Failure Correction Using Iterative Convex Optimization

Haiwei Song[1, 2, *], Guang Liang[1, 2], Wenbin Gong[2], and Jinpei Yu[1, 2]

Abstract—Element failure distorts the main-lobe pattern and increases side-lobe power level, which is almost impossible to be corrected artificially for space-borne array. It might be solved by redistributing the excitations of the left functional elements; however, this is a nonlinear, non-convex, and NP-hard problem. In this paper, two effective approaches are proposed for failure correction, which is performed for space-borne hexagonal array using digital beamforming (DBF). One method, a modified real-code genetic algorithm (RCGA), is employed that uses reinsertion and worst-elimination schemes, but it pays the high computation complexity. The other approach based on convex optimization chooses the excitations synthesized by RCGA as the initial points, and transforms the non-convex problem into a sequence of second-order cone programming (SOCP) problem, which can be solved iteratively by efficient optimization tool. Numerical results confirm that after the correction based on iterative convex optimization, the average root-mean-square error (RMSE) is reduced by 36%, and the relative side-lobe level (RSLL) is decreased by 6.7 dB, with respect to the RCGA-based correction pattern.

1. INTRODUCTION

Due to the advantage of high gain and wide coverage, space-borne array antenna has been employed in the global satellite communication system, such as Iridium and Globalstar system [1–3]. Space-borne array antenna is normally exposed to space environment that has extremely high/low temperatures and strong cosmic radiations, wherefore array elements will have the rising probability of failure as time goes by. Array symmetry may be destroyed by element failures, and sharp variations would be exerted in the field intensity across the array aperture. Consequently, the shaped beam pattern may be distorted with the increase of RSLL (the peak side-lobe level to the peak main-lobe level). To keep the availability of the space-borne array, the simplest solution is reduplicating the elements, however, a corresponding RF-channel is needed and both weight and complexity are increased.

So far, the methods of element failure correction can be classified into two categories: signal reconstruction approach and excitation redistribution approach. Signal reconstruction approach is that the output signals of some defective elements are reconstructed by output signals of the adjacent functional elements. Maillous employed an iterative reconstruction method based on the constant time delay between multiple array elements [4], and Levitas et al. developed a practical auto-compensation technique for element failure in active phased array [5]. One of the limitations of the first approach is that it must distinguish multiple arrival signal sources, and it becomes even more complicated for planar array. The second approach is redistributing the excitations of the remaining functional elements to form a new pattern, which approximates to the original pattern. Peters proposed a basic conjugate gradient algorithm to recalculate the weights of hexagonal array with some element failed [6]; however, it established an unconstrained optimization model, which only minimized the RSLL of failure array, and

Received 2 March 2014, Accepted 18 April 2014, Scheduled 14 May 2014

* Corresponding author: Haiwei Song (shw.phd@hotmail.com).

[1] Shanghai Institute of Microsystem and Information Technology, Chinese Academy of Science, China. [2] Shanghai Engineering Center for Microsatellites, China

other key metrics such as main-lobe width may not be satisfied. Intelligent algorithm, such as Genetic algorithm (GA) [7], particle swarm optimization (PSO) [8], bacteria foraging optimization (BFO) [9], support vector machine (SVM) [10], has been applied to array failure correction, and the mean squared error between the original pattern and correction pattern is typically selected as objective function of these algorithms. The main problem of these works is the high computation complexity, and it is quite difficult to implement them in the space-borne computer.

This paper adopts the excitation redistribution method based on iterative convex optimization, which can implement multiple constraints of pattern and have fast solving speed via interior-point algorithm [11]. In this paper, it is assumed that the output of defective element is zero, and all the proposed algorithms are performed on a 19-element hexagonal receiving array antenna with DBF. The outline of this study is listed below: Section 2 shows the gain pattern model of the hexagonal array, and meanwhile the shaped beam pattern synthesized by RCGA is given before element failures. In Section 3, element failure correction algorithm based on RCGA is firstly proposed, and then we develop a novel iterative convex programming-based correction algorithm with the initial excitations of RCGA. Section 4 provides the numerical simulation results. Finally, some meaningful conclusions are presented in Section 5.

2. SYSTEM DESCRIPTION

2.1. The Gain Pattern Model of Hexagonal Array Antenna

The geometry of receiving hexagonal array antenna with 19 elements is depicted in Figure 1. Element space is 0.545λ, where λ is the wavelength of the L-band sinusoidal wave. The array response $E(\theta, \varphi)$ can be written as:

$$E(\theta, \varphi) = \mathbf{w}^T \mathbf{a}(\theta, \varphi) = \sum_{i=1}^{19} I_i e^{j\alpha_i} e^{jk_0\psi_i} F_i(\theta, \varphi) \tag{1}$$

where θ and φ are the elevation and azimuth angle in the spherical coordinate, respectively. $k_0 = 2\pi/\lambda$ is the wave-number constant. $\psi_i = x_i u + y_i v$, where $u = \sin\theta\cos\varphi$ and $v = \sin\theta\sin\varphi$. x_i and y_i are x-coordinate and y-coordinate position of element i in Figure 1. I_i and α_i are amplitude and phase excitation of element i, respectively. $\mathbf{w}$ is complex excitation weight vector, and $\mathbf{w} = [w_1, w_2, \ldots, w_{19}]^T$. $\mathbf{a}(\theta, \varphi)$ is array manifold vector. $F_i(\theta, \varphi)$ is radiation pattern of individual element i, which is a dual-fed and dual-layer stacked patch antenna. Figure 2 shows three actual patterns of element 2, 8 and 15 at φ=90°, which is measured in spherical near-field anechoic chamber (Satimo) [12]. The space-borne hexagonal receiving array antenna employs the left hand circularly polarized (LHCP) mode, and the

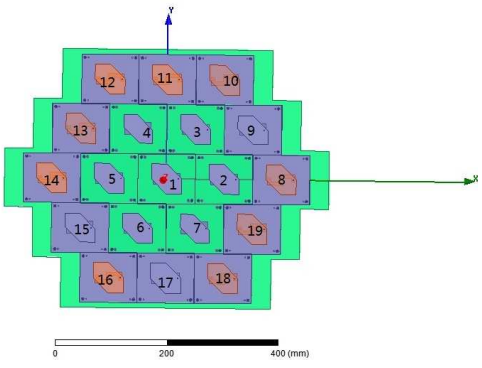

Figure 1. The geometry of hexagonal array.

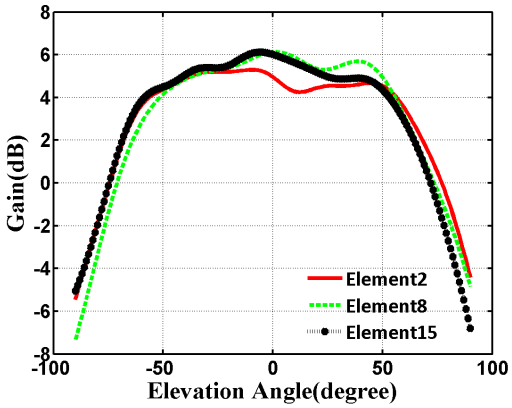

Figure 2. Measured pattern at $\varphi = 90°$.

normalized gain formula is given as follows:

$$G = \eta \frac{|E(\theta,\varphi)|^2}{\frac{1}{4\pi}\int_0^{\pi}\int_0^{2\pi}|E(\theta,\varphi)|^2 \sin\theta d\theta d\varphi} \tag{2}$$

where $\eta \approx 0.9$ is radiation efficiency.

2.2. The Shaped Beam Pattern Formed by RCGA

We employ this hexagonal array antenna to form seven shaped beam patterns which are mentioned in reference [13], and without loss of generality, failure correction is performed for the center beam pattern. The desired pattern gain $G_{d1}(\theta,\varphi)$ of center beam is defined as:

$$G_{d1}(\theta,\varphi) = \begin{cases} 10.5\,\text{dB} & 0 \le \theta \le 35^\circ,\ 0 \le \varphi \le 360^\circ \\ 0\,\text{dB} & \text{others} \end{cases} \tag{3}$$

Figure 3 shows the 3D desired gain pattern of center beam in u-v space. A RCGA-based pattern synthesis method is applied to minimize the mean-squared error between formed pattern and the desired pattern. The formed 3D pattern of center beam without element failure is depicted in Figure 4.

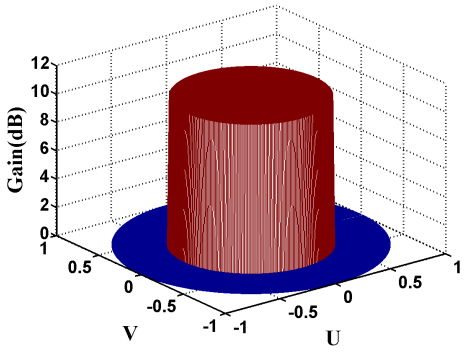

Figure 3. The 3D desired gain pattern.

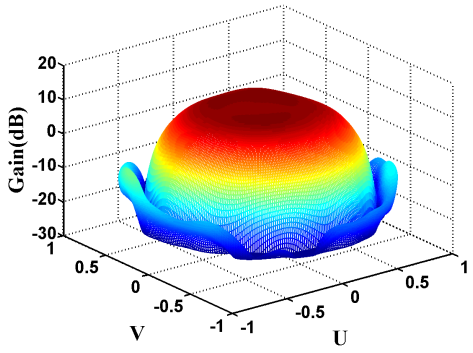

Figure 4. The shaped pattern from RCGA.

3. ELEMENT FAILURE CORRECTION ALGORITHM

3.1. RCCA-Based Element Failure Correction Algorithm

When the ith element is completely failed, it is equivalent to $I_i = 0$, $\alpha_i = 0$ in formula (1). RCGA has been applied to synthesize functional beam pattern, and naturally we employ RCGA to correct element failures. The fitness function of RCGA-based failure correction algorithm is defined as:

$$f(\boldsymbol{I},\boldsymbol{\alpha}) = \sum_{m=1}^{N_\theta}\sum_{n=1}^{N_\varphi}\left(G(\theta_m,\varphi_n) - G_{d1}(\theta_m,\varphi_n)\right)^2 \tag{4}$$

where N_θ and N_φ are the numbers of samples in the elevation plane and azimuth plane. $G(\theta_m,\varphi_n)$ is the beam gain pattern formed by the remaining functional elements. I_i' and α_i' are the excitations of the functional ith element's amplitude and phase, which is selected as a gene, and the float value of element excitation is acted as gene encoding. The chromosome structure is defined as: $(I_1', I_2', \ldots, I_N', \alpha_1', \alpha_2', \ldots, \alpha_N')$, where N is the number of the left functional elements.

Besides the solving precision improvement via real code, we also use two improved methods in RCGA-based failure correction algorithm: reinsertion and worst-elimination methods. Reinsertion method was firstly proposed by De Jong [14], which assumes that a generation gap (GGAP) exists

between parents and offspring and that fewer individuals are produced by GA operation than the size of the original population. The individuals in the old population would be replaced by the new individual with the better fitness, and then some elitist individuals will survive in the successive generations. The second method is proposed by this paper, where the individuals are sorted with the fitness firstly, and the last two individuals are eliminated by two new initialized individuals. The advantage of worst-elimination method is that the inferior solution is removed and randomness increased. The flowchart of RCGA-based element failure correction algorithm is depicted in Figure 5, where MAXG means the maximum number of generations, and stochastic universal sampling (SUS) is selection operator. Intermediate recombination (IntRec) is real code crossover operator in our algorithm.

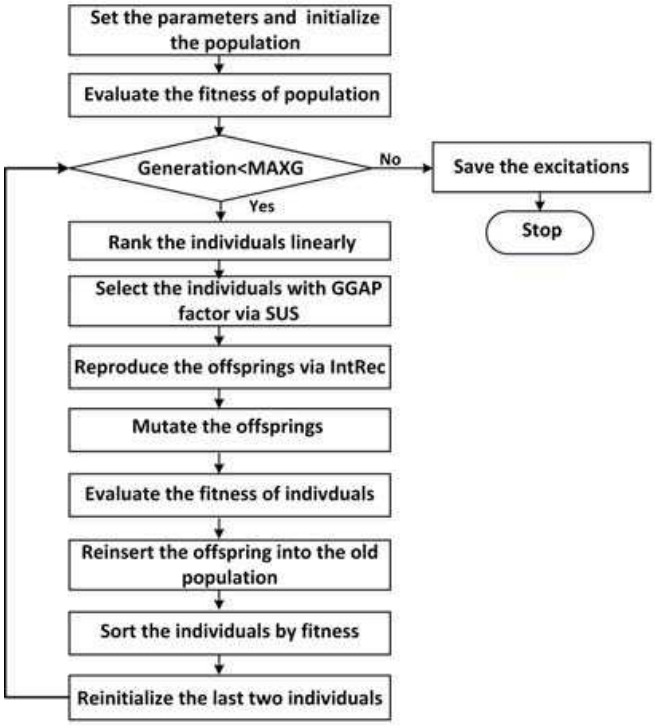

Figure 5. The flowchart of RCGA-based failure correction algorithm.

3.2. Element Failure Corrected by Iterative Convex Programming

We remove the constant factor and do not normalize the gain in formula (2), and then the failure correction problem is given as the following optimization problem:

$$\min_{\mathbf{w}} \varepsilon$$

$$s.t. \quad \left|\left|\mathbf{w}^T\mathbf{a}'(\theta_m,\varphi_n)\right|^2 - G'_d(\theta_m,\varphi_n)\right| \le \varepsilon, \quad (\theta_m,\varphi_n)\in ML, \ m=1,\ldots,M_b, \quad n=1,\ldots,N_b \tag{5a}$$

$$\left|\mathbf{w}^T\mathbf{a}'(\theta_s,\varphi_q)\right| \le \zeta \qquad (\theta_s,\varphi_q)\in SL, \quad s=1,\ldots,S_b, \quad q=1,\ldots,Q_b \tag{5b}$$

where ζ is a fixed side-lobe level, and ε is a slack variable, which controls the error level. $\mathbf{a}'(\theta,\varphi)$ is the array manifold vector of the left functional elements. ML and SL are the regions of main-lobe and side-lobe. ML region contains M_b sample points in θ and N_b sample points in φ , and the sample grid in SL region is $S_b \times Q_b$ for (θ,φ). $G'_d(\theta,\varphi)$ is the non-failure gain pattern, which can be calculated by: $G'_d(\theta,\varphi) = |\mathbf{w}_d^T\mathbf{a}(\theta,\varphi)|^2$. $\mathbf{w}_d$ is the element excitation vector synthesized by RCGA algorithm without element failures, as is mentioned in Section 2. The value of $\mathbf{w}_d$ is given in Table 1.

The low bound of constraint (a) is non-convex, thus the optimization problem (5) cannot be directly solved by convex optimization method. We use multiconvex inequality condition [15, 16], which

Table 1. The excitations of pattern with no failure.

amplitude excitations	$\boldsymbol{I_1}$	$\boldsymbol{I_2}$	$\boldsymbol{I_3}$	$\boldsymbol{I_4}$	$\boldsymbol{I_5}$	$\boldsymbol{I_6}$	$\boldsymbol{I_7}$	$\boldsymbol{I_8}$	$\boldsymbol{I_9}$	$\boldsymbol{I_{10}}$
	4.9973	4.5119	4.9859	4.9961	2.7205	2.0448	2.4407	1.4833	1.2739	1.7414
	$\boldsymbol{I_{11}}$	$\boldsymbol{I_{12}}$	$\boldsymbol{I_{13}}$	$\boldsymbol{I_{14}}$	$\boldsymbol{I_{15}}$	$\boldsymbol{I_{16}}$	$\boldsymbol{I_{17}}$	$\boldsymbol{I_{18}}$	$\boldsymbol{I_{19}}$	
	1.5280	1.3948	1.2859	1.0019	1.3746	1.3146	1.0400	1.0020	1.4544	
phase excitations	$\boldsymbol{\alpha_1}$	$\boldsymbol{\alpha_2}$	$\boldsymbol{\alpha_3}$	$\boldsymbol{\alpha_4}$	$\boldsymbol{\alpha_5}$	$\boldsymbol{\alpha_6}$	$\boldsymbol{\alpha_7}$	$\boldsymbol{\alpha_8}$	$\boldsymbol{\alpha_9}$	$\boldsymbol{\alpha_{10}}$
	3.7130	3.6252	3.6426	3.6616	3.6731	4.2518	3.3229	1.3419	4.0547	4.9868
	$\boldsymbol{\alpha_{11}}$	$\boldsymbol{\alpha_{12}}$	$\boldsymbol{\alpha_{13}}$	$\boldsymbol{\alpha_{14}}$	$\boldsymbol{\alpha_{15}}$	$\boldsymbol{\alpha_{16}}$	$\boldsymbol{\alpha_{17}}$	$\boldsymbol{\alpha_{18}}$	$\boldsymbol{\alpha_{19}}$	
	3.8680	1.7421	2.1513	6.2813	0.1182	0.2739	0.0212	6.2820	1.4264	

introduces two optimization variables: $\mathbf{w}_1$ and $\mathbf{w}_2$, wherefore the re-synthesized gain pattern is expressed as $|\mathbf{w}_1^T\mathbf{a}'(\theta,\varphi)+\mathbf{w}_2^T\mathbf{a}'(\theta,\varphi)|^2$. The relaxing process of low bound is given as follows:

$$\begin{aligned}&\left|\mathbf{w}_1^T\mathbf{a}'(\theta,\varphi)+\mathbf{w}_2^T\mathbf{a}'(\theta,\varphi)\right|^2 \geq 4\mathrm{Re}\left\{\left(\mathbf{w}_1^T\mathbf{a}'\left(\theta_m,\varphi_n\right)\right)^*\left(\mathbf{w}_2^T\mathbf{a}'\left(\theta_m,\varphi_n\right)\right)\right\}\\ \Rightarrow\ &4\mathrm{Re}\left\{\left(\mathbf{w}_1^T\mathbf{a}'\left(\theta_m,\varphi_n\right)\right)^*\left(\mathbf{w}_2^T\mathbf{a}'\left(\theta_m,\varphi_n\right)\right)\right\} \geq \max\left\{G'_d(\theta_m,\varphi_n)+\varepsilon,0\right\}. \end{aligned} \tag{6}$$

When $\mathbf{w}_1$ is fixed, the inequalities (6) is convex in variable $\mathbf{w}_2$, hence the problem (5) can be solved alternately over $\mathbf{w}_1$ and $\mathbf{w}_2$ by convex programming method.

SOCP is a typical subclass of convex optimization method, and the problem (5) can be written as the form of SOCP. It is assumed that $\mathbf{w}_1$ is fixed, and then we define the solution vector $\mathbf{y}=[\varepsilon,\mathrm{Re}(\mathbf{w}_2)^T,\mathrm{Im}(\mathbf{w}_2)^T]^T$, where $\mathrm{Re}(\mathbf{w}_2)$ and $\mathrm{Im}(\mathbf{w}_2)$ are real part and imaginary part vector of $\mathbf{w}_2$, respectively. Let $\mathbf{b}=[-1,\mathbf{0}_{1\times N},\mathbf{0}_{1\times N}]^T$, and then the primal SOCP problem of (5) is written as the follow standard dual SOCP problem:

$$\begin{aligned}&\max_{\mathbf{y}}\ \mathbf{b}^T\mathbf{y}\\ &s.t.\quad c_i-\mathbf{A}_i^T\mathbf{y}\in\Re_+,\ \ i=1,\ldots,MN &\text{(7a)}\\ &\qquad \mathbf{c}_{1+MN+j}-\mathbf{A}_{1+MN+j}^T\mathbf{y}\in Qcone_j^4,\ \ j=1,\ldots,MN &\text{(7b)}\\ &\qquad \mathbf{c}_{1+2MN+k}-\mathbf{A}_{1+2MN+k}^T\mathbf{y}\in Qcone_{k+MN}^3,\ \ k=1,\ldots,SQ &\text{(7c)}\end{aligned}$$

where constraint (7a) is a linear constraint, and $\Re_+$ represents non-negative real number cone. MN is the total number of linear constraint, and $MN=M_b\times N_b$. Both c_i and $\mathbf{A}_i$ have two values conditioned by the size relation between $G'_d(\theta_i,\varphi_i)$ and ε. When $G'_d(\theta_i,\varphi_i)\geq\varepsilon$, $c_i=-G'_d(\theta_i,\varphi_i)$ and $\mathbf{A}_i=-[1,4\mathrm{Re}(\mathbf{u}(\theta_i,\varphi_i))^T,-4\mathrm{Im}(\mathbf{u}(\theta_i,\varphi_i))^T]^T$, and otherwise $c_i=0$ and $\mathbf{A}_i=-[0,4\mathrm{Re}(\mathbf{u}(\theta_i,\varphi_i))^T,-4\mathrm{Im}(\mathbf{u}(\theta_i,\varphi_i))^T]^T$, where $\mathbf{u}(\theta,\varphi)=(\mathbf{w}_1^T\mathbf{a}'(\theta,\varphi))^*\mathbf{a}(\theta,\varphi)$.

Constraint (7b) is a quadratic constraint, and $Qcone^4$ means the second-order cone with 4 dimensions. This constraint is derived from the upper bound constraint of (5a). $\mathbf{c}_{1+MN+j}$ and $\mathbf{A}_{1+MN+j}$ are given by:

$$\mathbf{c}_{1+MN+j}=\begin{bmatrix}G'_d\left(\theta_j,\varphi_j\right)+1\\ 2\mathrm{Re}\left(\mathbf{w}_1^T\mathbf{a}'\left(\theta_j,\varphi_j\right)\right)\\ 2\mathrm{Im}\left(\mathbf{w}_1^T\mathbf{a}'\left(\theta_j,\varphi_j\right)\right)\\ G'_d\left(\theta_j,\varphi_j\right)-1\end{bmatrix},\qquad \mathbf{A}_{1+MN+j}=-\begin{bmatrix}1, & \mathbf{0}_{1\times N} & \mathbf{0}_{1\times N}\\ 0, & 2\mathrm{Re}(\mathbf{a}'\left(\theta_j,\varphi_j\right))^T, & -2\mathrm{Im}(\mathbf{a}'\left(\theta_j,\varphi_j\right))^T\\ 0, & 2\mathrm{Im}(\mathbf{a}'\left(\theta_j,\varphi_j\right))^T, & 2\mathrm{Re}(\mathbf{a}'\left(\theta_j,\varphi_j\right))^T\\ 1, & \mathbf{0}_{1\times N} & \mathbf{0}_{1\times N}\end{bmatrix}^T.$$

Constraint (5b) can be formulated as constraint (7c). $Qcone^3$ represents the quadratic cone with 3 dimensions. $\mathbf{c}_{1+2MN+k}$ and $\mathbf{A}_{1+2MN+k}$ are written as:

$$\mathbf{c}_{1+2MN+k}=\begin{bmatrix}\zeta\\ \mathrm{Re}\left(\mathbf{w}_1^T\mathbf{a}'\left(\theta_k,\varphi_k\right)\right)\\ \mathrm{Im}\left(\mathbf{w}_1^T\mathbf{a}'\left(\theta_k,\varphi_k\right)\right)\end{bmatrix},\quad \mathbf{A}_{1+2MN+k}=-\begin{bmatrix}0, & 0, & 0\\ 0, & \mathrm{Re}(\mathbf{a}'\left(\theta_k,\varphi_k\right))^T, & -\mathrm{Im}(\mathbf{a}'\left(\theta_k,\varphi_k\right))^T\\ 0, & \mathrm{Im}(\mathbf{a}'\left(\theta_k,\varphi_k\right))^T, & \mathrm{Re}(\mathbf{a}'\left(\theta_k,\varphi_k\right))^T\end{bmatrix}^T.$$

Problem (7) can be directly solved by those highly efficient optimization software packages, such as SeDuMi [17]. Note that we only seek the local minima by the iterative SOCP, and the initial point highly affects the optimal solution. In (7), we set $\mathbf{w}_1$=$\mathbf{w}'_d/2$, where $\mathbf{w}'_d$ is the excitations coefficients listed in Table 1 except the excitations of failed elements. The reason is that the beamforming weights of the left remaining elements have been stored in memory previously, and no extra computation complexity is added for initialization, and moreover RCGA-based pattern synthesis algorithm is a global optimization pattern synthesis algorithm and offers a promising initial points even though some elements fail. Additionally, two conditions lie in constraint (7a), and ε must be initialized in the iterative optimization process. In the first iteration, ε is calculated as:

$$\varepsilon = \max \left| \left| (\mathbf{w}'_d)^T \mathbf{a}'(\theta, \varphi) \right|^2 - G'_d(\theta, \varphi) \right|. \tag{8}$$

And in the next step, ε is initialized by $\mathbf{y}(1)$, which is the first component of the solution vector. The flowchart of iteration convex programming-based failure correction algorithm is given as in Figure 6, where MAXI represents the maximal number of the iterations.

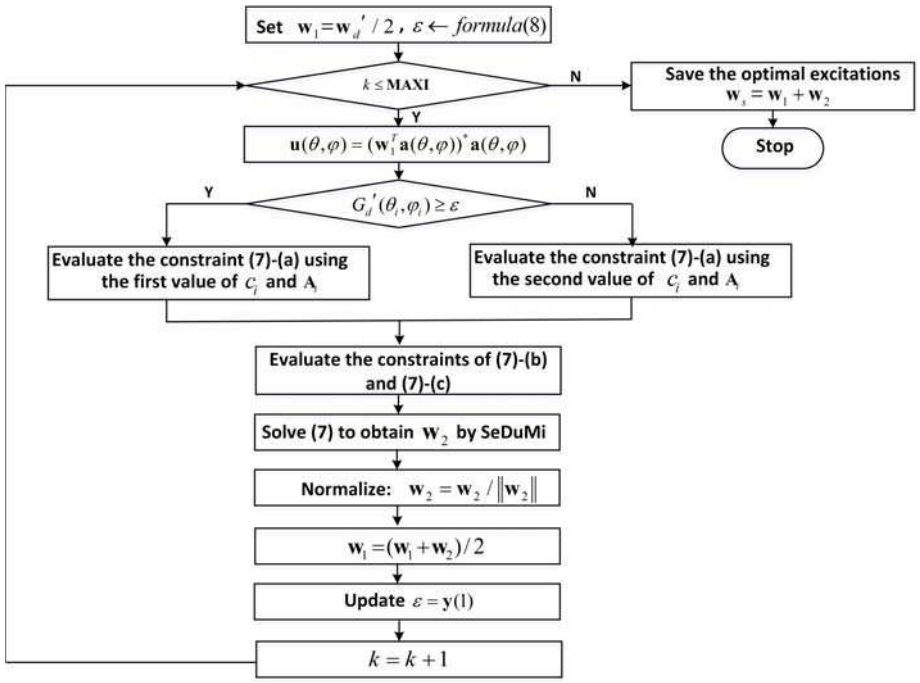

Figure 6. The flowchart of iterative convex programming-based failure correction algorithm.

4. NUMERICAL RESULTS

This paper only takes the effect of one element failure into account, and comparing the values of RMSE between the pattern with an element failure and the functional pattern, the gain decrease after element 2 failure is greater than that of other element failure, so the corrected algorithm is used in view of the failure of element 2.

The parameters used in RCGA-based correction algorithm are given as follows: a) the population size is 200, and the maximum number of generations is 250. b) GGAP factor is 0.96. c) the crossover probability is 0.9. d) the mutation probability is 0.15. e) $N_\theta = 180$ and $N_\varphi = 360$. In iterative convex programming (ICP)-based failure correction algorithm, the parameters are set as: a) the SLL threshold $\zeta = -9\,\text{dB}$. b) the constraint domain of the main-lobe width is $0^\circ \le \theta \le 65^\circ$ and $0^\circ \le \varphi \le 360^\circ$, wherefore $M_b = 65$ and $N_b = 360$. The side-lobe constraint domain is $66^\circ \le \theta \le 180^\circ$ and $0^\circ \le \varphi \le 360^\circ$, and hence $S_b = 115$, $Q_b = 360$.

Figure 7 and Figure 8 present the 3D pattern corrected by RCGA and ICP, respectively. From these two figures, we can see that the 3D shape of the ICP-based correction (ICPC) pattern is closer to the pattern with no element failure depicted in Figure 4, with respect to 3D pattern after RCGA correction. The sectional gain patterns are compared at $\varphi = 0°$, $\varphi = 90°$ and $\varphi = 120°$, which are shown in Figure 9, Figure 10 and Figure 11, respectively. It is apparent from the three figures that after element 2 failure, the main-beam width is broadened and the side-lobe level elevated. Both the RCGA-based correction (RCGAC) pattern and ICPC pattern improve the performance of failure pattern; however, the ICPC algorithm achieves a lower RSLL and smaller difference, than the RCGAC algorithm.

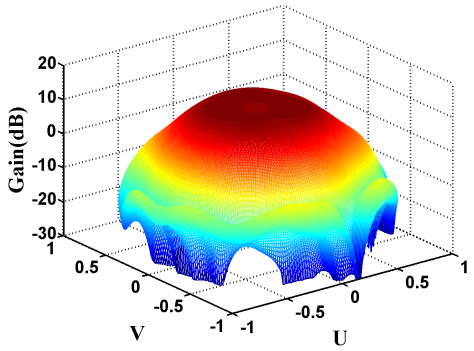

Figure 7. 3D pattern corrected by RCGA.

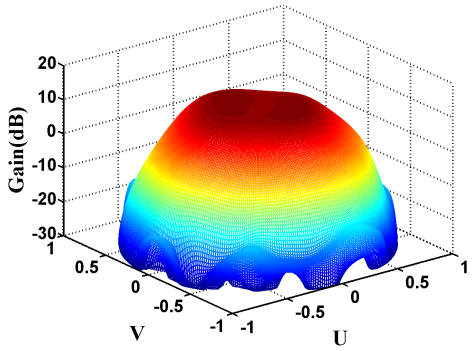

Figure 8. 3D pattern corrected by ICP.

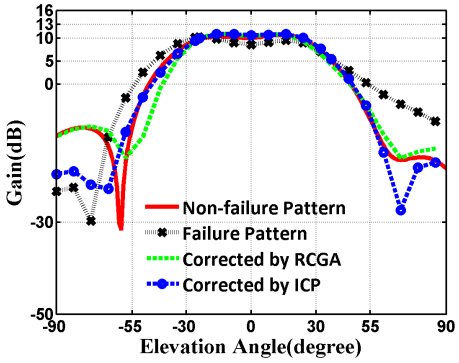

Figure 9. The sectional patterns at $\varphi = 0°$.

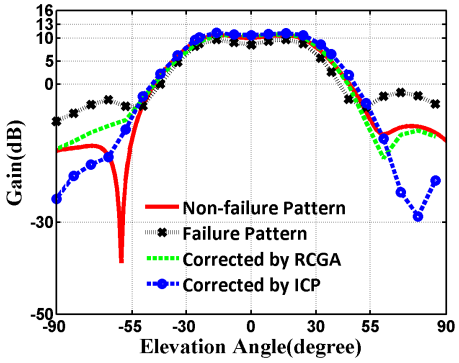

Figure 10. The sectional patterns at $\varphi = 90°$.

The comparison of RMSE is performed for the failure pattern, RCGAC pattern, and the ICPC pattern, depicted in Figure 12. It is indicated that the RMSE value of failure pattern across the whole azimuth domain is greater than that of ICPC pattern, and meanwhile the RMSE fluctuation range of ICPC pattern is less than that of RCGAC pattern. Figure 13 and Figure 14 present the comparison for the RSLL and the half power beam-width in θ dimension (θ-HPBW) towards different patterns. Clearly, the best performance of side-lobe suppression for correction pattern is achieved by ICPC algorithm, and RCGAC algorithm barely improves the value of RSLL. θ-HPBW is fluctuated dramatically after the element failure, and both the correction algorithms narrow the fluctuation range of θ-HPBW, but the fluctuation is more stationary for ICPC algorithm.

The mean RMSE (MRMSE) across the whole azimuth domain is expressed as:

$$\text{MRMSE} = \frac{\sum_{i=1}^{M_\varphi} \sqrt{\left(\sum_{j=1}^{M_\theta} \left(G(\theta_j, \varphi_i) - G_i(\theta_j, \varphi_i)\right)^2\right) \Big/ M_\theta}}{M_\varphi}$$

where $\varphi_i \in [0°, 360°]$ and $\theta_j \in [-55°, 55°]$. As shown in Table 2, four pattern's quantitative metrics, MRMSE, the mean RSLL (MRSLL) and the mean θ-HPBW, are listed. It is clearly seen that the

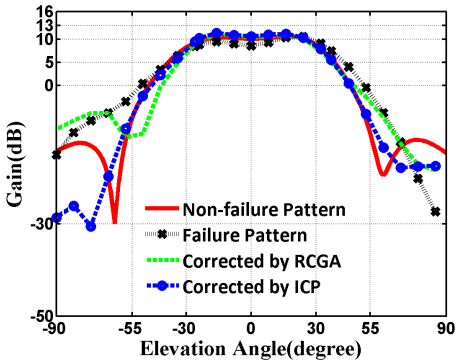

Figure 11. Sectional patterns at $\varphi' = 120°$.

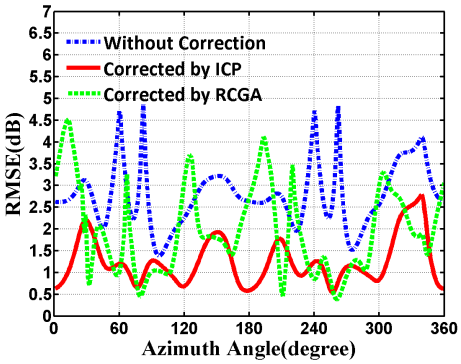

Figure 12. The comparison of RMSE.

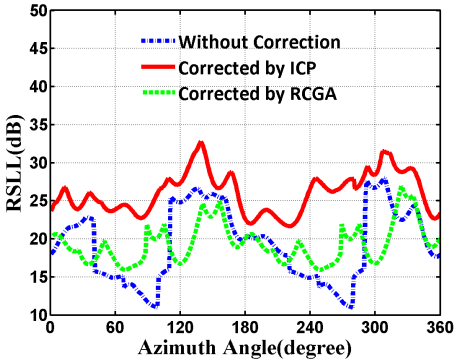

Figure 13. The comparison of RSLL.

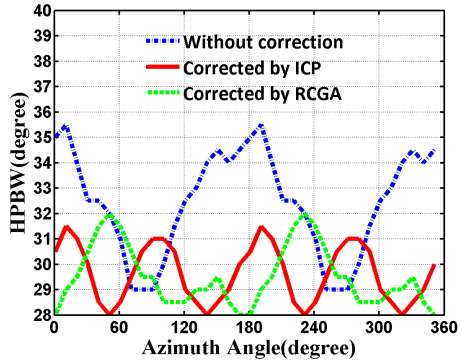

Figure 14. The comparison of θ-HPBW.

MRMSE value after ICPC algorithm is improved by as much as 55% and 36%, compared to the one without correction and the one from RCGAC algorithm, respectively. The decrease of the mean RSLL of ICPC algorithm is 6.77 dB and 6.71 dB, with respect to the value from failure pattern and RCGAC pattern. The improvement of θ-HPBW is almost equal for the two correction algorithms. Although the HPBW's domain of the desired pattern is $0° \leq \theta \leq 35°$, the practical requirement for 7-beam coverage is $0° \leq \theta \leq 30°$ due to the gain overlap among multiple beams. Overall, the performance of HBPW of ICPC pattern is acceptable.

Table 2. The performance comparison of different pattern.

Pattern	MRMSE (dB)	MRSLL (dB)	Mean HPBW (°)
Pattern with no failure	0	−20.66	31.18
Pattern with an failure	2.78	−19.29	32.42
RCGAC pattern	1.97	−19.35	29.53
ICPC pattern	1.26	−26.06	29.68

5. CONCLUSION

This paper focuses on the adverse effects of element failure for space-borne hexagonal array antenna. RCGA-based correction algorithm is firstly employed and proved to narrow the difference between the desired pattern and the re-synthesized pattern with an element failure. However, it is a computation-intensive algorithm and unpractical to implement on the poor space-borne computer. Initializing with the stored beamforming weights of the left functional elements, iterative convex programming-based correction algorithm abandons the time-consuming computation, and decomposes the complex non-

convex problem into a sequence of fast solved SOCP problem. The results show that the correction pattern from iterative convex programming is superior to that from RCGA correction, which provides a feasible method of element failure correction implemented on board. The current work depends on desktop software, future research might implement the interior point algorithm on space-borne computer.

ACKNOWLEDGMENT

The work was supported by Innovation foundation of Chinese Academy of Sciences (No. CXJJ-11-S107) and Natural Science Foundation of Shanghai city (11ZR1435000).

REFERENCES

1. Rohwer, A. B., D. H. Desrosiers, W. Bach, et al., "Iridium main mission antennas: A phased array success story and mission update," *IEEE International Symposium on Phased Array Systems and Technology*, 504–511, 2010.
2. Croq, F., E. Vourch, M. Reynaud, et al., "The Globalstar 2 antenna sub-system," *3rd European Conference on Antennas and Propagation*, 598–602, 2009.
3. Liang, G., W. Gong, H. Liu, et al., "Development of 61-channel digital beam-forming (DBF) transmitter array for mobile satellite communication," *Progress In Electromagnetics Research*, Vol. 97, 175–195, 2009.
4. Mailloux, R. J., "Array failure correction with a digital beamformed array," *IEEE Transactions on Antennas and Propagation*, Vol. 44, No. 12, 1543–1550, 1996.
5. Levitas, M., D. A. Horton, and T. C. Cheston, "Practical failure compensation in active phased arrays," *IEEE Transactions on Antennas and Propagation*, Vol. 47, No. 3, 524–535, 1999.
6. Peters, T. J., "A conjugate gradient-based algorithm to minimize the sidelobe level of planar arrays with element failures," *IEEE Transactions on Antennas and Propagation*, Vol. 39, No. 10, 1497–1504, 1991.
7. Mitilineos, S. A. and C. N. Capsalis, "On array failure mitigation using genetic algorithms and a priori joint optimization," *IEEE Transactions on Antennas and Propagation*, Vol. 47, No. 5, 227–232, 2005.
8. Yeo, B. K. and Y. Lu, "Fast array failure correction using improved particle swarm optimization," *Apmc: 2009 Asia Pacific Microwave Conference*, Vol. 1, 1537–1540, 2009.
9. Acharya, O. P., A. Patnaik, and B. Choudhury, "Fault finding in antenna arrays using bacteria foraging optimization technique," *National Conference on Communications (NCC)*, 1–5, 2011.
10. Zhao, H., Y. Zhang, E. Li, et al., "Diagnosis of array failure in impulsive noise environment using unsupervised support vector regression method," *IEEE Transactions on Antennas and Propagation*, Vol. 61, No. 11, 5508–5516, 2013.
11. Lebret, H. and S. Boyd, "Antenna array pattern synthesis via convex optimization," *IEEE Transactions on Signal Processing*, Vol. 45, No. 3, 526–532, 1997.
12. Microwave Vision Group, *Antenna Measurement and Radome Test System*, MVG-EBOOK, 2013.
13. Song, H., G. Liang, W. Gong, et al., " Performance analysis of a seven-beam CDMA-based LEO satellite system," *IEEE Asia-Pacific Conference on Antennas and Propagation*, 174–175, 2012.
14. Kenneth, A., J. De, A. D. Kenneth, et al., "Generation gaps revisited," *Foundations of Genetic Algorithms*, 1992.
15. Wang, F., V. Balakrishnan, P. Y. Zhou, et al., "Optimal array pattern synthesis using semidefinite programming," *IEEE Transactions on Signal Processing*, Vol. 51, No. 5, 1172–1183, 2003.
16. Fuchs, B., A. Skrivervik, and J. R. Mosig, "Shaped beam synthesis of arrays via sequential convex optimizations," *IEEE Antennas and Wireless Propagation Letters*, Vol. 12, 1049–1052, 2013.
17. Sturm, J. F., "Using SeDuMi 1.02, A matlab toolbox for optimization over symmetric cones," *Optimization Methods and Software*, Vol. 11, No. 12, 625–653, 1999.